Interaction of spherical colloidal particles in nematic media with degenerate planar anchoring

Mohammad Reza Mozaffari,[a] Mehrtash Babadi,[b] Jun-ichi Fukuda[c] and Mohammad Reza Ejtehadi*[a]

Received 2nd August 2010, Accepted 4th October 2010
DOI: 10.1039/c0sm00761g

The interaction between two spherical colloidal particles with degenerate planar anchoring in a nematic media is studied by numerically minimizing the bulk Landau–de Gennes and surface energy using a finite element method. We find that the energy achieves its global minimum when the particles are in close contact and forming an angle $\theta = 28^\circ \pm 2$ with respect to the bulk nematic director, in agreement with the experiments. Although the quadrupolar structure of the director field is preserved in the majority of configurations, we show that for smaller orientation angles and at smaller inter-particle separations, the axial symmetry of the topological defect-pairs is continuously broken, resulting in the emergence of an attractive interaction.

1 Introduction

Studying the behavior of colloidal particles in anisotropic fluids with long-range orientational ordering, such as nematic liquid crystals, has attracted great attention in soft condensed matter physics.[1–6] The orientation order parameter of the fluid (*e.g.* director of nematic liquid crystal) is distorted from its uniform orientation in the bulk due to anchoring on the surface of the colloidal particles. These elastic distortions create topological defects around the particles[7] and induce anisotropic long and short range interactions between the particles.[8,9]

Depending on the colloidal material and its coating, the surrounding fluid may have a normal orientation (*normal or homeotropic anchoring*), or parallel orientation (*planar anchoring*) with respect to the colloidal surfaces. For strong normal anchoring, the orientation of the fluid is locally and uniquely determined on the colloidal surfaces. For planar anchoring, the orientation of the fluid is degenerate on the colloidal surfaces and is determined by the global structure of the fluid. Although the director field on the surface of the particles is affected by the environment for any finite anchoring strength of either type, the extra local degeneracy of planar anchorings makes their theoretical investigations more complicated.

In the case of a single colloidal particle, the particle-defect pair induces a dipolar or a quadrupolar long-range elastic distortion field[10,11] depending on the anchoring type. The long-range dipolar structure results from a *satellite* point defect, when the size of the particle is large compared to the coherence length of the nematic fluid and the anchoring is normal.[7,9] The quadrupolar configuration appears in both normal and planar anchorings. In the normal case, a disclination ring (*Saturn ring*) encircles the particle, when the size of the particle is small or the strength of anchoring is weak.[7,8] In planar anchoring, the elastic distortions form two point defects (*boojums*) at the poles of the particles, aligned along the nematic direction.[7,8]

The more physically interesting configurations are achieved when there are many colloidal particles present in the medium. For large separations of particles, the defects around of each of the particles are independent of those of the other particles, and (anisotropic) interaction potential between them is determined by the long-range orientational field of the fluid. In this regime, and in the case of two particles separated by a distance d, the effective interaction potential between them is proportional to d^{-3} or d^{-5} for dipolar or quadrupolar defect configurations, respectively.[1,3,7,8] When the particles approach each other, the defect structures are distorted and the interactions deviate from the far-field dipolar–dipolar or quadrupolar–quadrupolar interactions.[12–18]

Experimentally, the colloidal interactions in nematic liquid crystals are studied using optical[4] or magneto-optical tweezers.[19,20] The medium-induced interactions play an essential role in the formation of chain[4] or crystal[2,21,22] suspensions of the colloids (or droplets) in nematic liquid crystals.

Smalyukh *et al.*[4] have measured the angular and the radial components of the force between two particles with planar anchoring in a nematic liquid crystal as a function of the inter-particle separation d and the angle between the bulk nematic

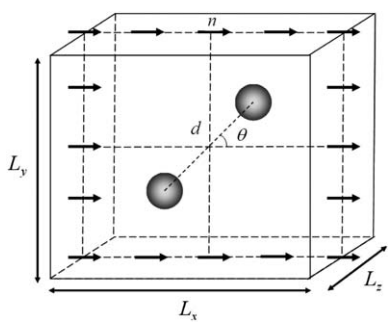

Fig. 1 A schematic representation of the studied system. The nematic director is fixed in the x direction at the boundaries and two particles are symmetrically placed in x–y plane with respect to the center of the box.

[a]*Department of Physics, Sharif University of Technology, P.O. Box 14588-89694, Tehran, Iran. E-mail: ejtehadi@sharif.edu*
[b]*Department of Physics, Harvard University, Cambridge, MA, 02138, USA*
[c]*Nanosystem Research Institute, National Institute of Advanced Industrial Science and Technology (AIST), 1-1-1 Umezono, Tsukuba, 305-8568, Japan*

director with the vector connecting the particles, θ (see Fig. 1). They observe deviation from the far-field theoretical quadrupole-quadrupole interaction[8] when the objects are in the close-contact regime. They also find that the equilibrium configuration corresponds to a very small separation of particles, $d \simeq 2R$, and $\theta \simeq 30^\circ$.

In this paper, we study the fluid-induced interaction between two spherical colloidal particles of radius R by numerically minimizing the sum of elastic Landau–de Gennes free energy of the bulk fluid[23] and the degenerate planar anchoring surface energy introduced by Fournier and Galatola[24] In particular, we are interested in the regime of strong anchoring and large particles (R is large compared to the coherence length of the fluid, ξ). Our main goal is to study the close-contact configurations for which no theoretical work has been done to our knowledge, though interesting physics is expected to emerge due to the strong interaction of the topological defects. We also aim to explain the experimentally observed angle of $\theta \simeq 30^\circ$ at equilibrium.

The paper is organized as follows. The theoretical model is explained in Section 2. We describe the details of our numerical approach in Section 3. We finally present and discuss the results in Section 4 and summarize our findings in Section 5.

2 The model

The geometry of the studied system is schematically illustrated in Fig. 1. We consider two identical spherical colloidal particles with radius R immersed in a 3D nematic cell. The nematic director is aligned along the x-axis at the boundaries of the cell. We scale all the lengths with respect to the radius of the particles. The dimensions of the cell is $L_x = 15R$, $L_y = 15R$ and $L_z = 6R$. The centers of the particles are confined to the plane $z = L_z/2$ and are separated by a center-to-center distance d. The line joining the center of the particles makes an angle θ with x-axis. The dimensions of the cell are chosen in a way to ensure that in all of the studied configurations, the distance between the boundaries and the particles is much larger than the coherence length and also large enough so that the nematic director distribution is not affected by the boundaries. The free energy of the system can be written as:

$$F(d, \theta) = F_b(d, \theta) + F_s(d, \theta) + F_{c-c}(d) \quad (1)$$

where $F_b(d, \theta)$ is bulk nematic fluid free energy, $F_s(d, \theta)$ is the surface energy and $F_{c-c}(d)$ is the Van der Waals colloid-colloid interaction. The free energy functionals will be described in detail in the following sections.

In realistic situations, the only appreciable effect of Van der Waals colloid–colloid interactions is to provide a short-range repulsion between the colloidal particles. Such effects become relevant only in the regime where the separation of the colloid surfaces approaches the atomic length-scales. In this study, we confine ourselves to the regime where the surface separations are larger than the nematic coherence length, *i.e.* $d - 2R \gg \xi \gg 1$ Å. We note that the surface separations can chosen to be appreciably smaller than the size of the particles in this regime. Therefore, due to the separation of scales in this regime, we ignore the Van der Waals interaction between the colloids in this study.

2.1 The nematic order parameter

The nematic fluid is described by a local, 3 × 3, traceless and symmetric tensor order parameter, $Q_{ij} = S(\hat{n}_i\hat{n}_j - \delta_{ij}/3)$, which can be specified by five independent components,

$$\boldsymbol{Q} = \begin{pmatrix} Q_{11} & Q_{12} & Q_{13} \\ Q_{12} & Q_{22} & Q_{23} \\ Q_{13} & Q_{23} & Q_{33} \end{pmatrix} \quad (2)$$

where $Q_{33} = -(Q_{11} + Q_{22})$. The scalar order parameter, S, and the director orientation, $\hat{n}$, are locally obtained by the largest eigenvalue of the tensor order parameter, $\lambda_{max} = \frac{2}{3}S$, and its corresponding eigenvector, respectively. We note that working with a tensor order parameter and expanding the free energy in its terms allows the formation of biaxial order, which is a necessary ingredient for a realistic description of topological defects and their interactions.

2.2 The bulk free energy

The bulk free energy of the nematic fluid is described well by the Landau–de Gennes model,[23] in which the free energy functional is expanded in powers of the tensor order parameter and its spatial derivatives:

$$F_b = \int_\Omega dV \left(\frac{A}{2}Q_{ij}Q_{ji} - \frac{B}{3}Q_{ij}Q_{jk}Q_{ki} + \frac{C}{4}(Q_{ij}Q_{ji})^2 + \frac{L_1}{2}\partial_k Q_{ij}\partial_k Q_{ij} + \frac{L_2}{2}\partial_j Q_{ij}\partial_k Q_{ik} \right) \quad (3)$$

where the indices refer to Cartesian coordinates, the summation over repeated indices is assumed and Ω denotes the volume occupied by the nematic liquid crystal. The first three terms are the Landau–de Gennes free energy which describe the bulk isotropic–nematic (IN) transition. The coefficients A, B, and C are the material-dependent parameters.

The derivative terms are the contribution of the elastic free energy in the nematic phase. The nematic elastic constants, L_1 and L_2, are related to the Frank elastic constants by $L_1 = K_{twist}/2S^2$ and $L_2 = (K_{splay} - K_{twist})/2S^2 = (K_{bend} - K_{twist})/2S^2$. In this study we restrict ourselves to one-elastic constant approximation that means all the Frank elastic constants should be equivalent which leads to $L_2 = 0$.

To simplify calculations, we rescale the tensor order parameter as $q = (4B/3\sqrt{6}C)^{-1}Q$, such that $q_{ij} = \hat{S}(\hat{n}_i\hat{n}_j - \delta_{ij}/3)$, where $\hat{S} = (4B/3\sqrt{6}C)^{-1}S$. As a consequence, the dimensionless free energy becomes

$$\hat{f}_b = \frac{F_b}{f_0 R^3} = \int_\Omega d\hat{V} \left(\frac{\tau}{2}q_{ij}q_{ji} - \frac{\sqrt{6}}{4}q_{ij}q_{jk}q_{ki} + \frac{1}{4}(q_{ij}q_{ji})^2 + \frac{1}{2}\hat{\xi}^2\hat{\partial}_k q_{ij}\hat{\partial}_k q_{ij} \right) \quad (4)$$

where $f_0 = C(4B/3\sqrt{6}C)^4$, $\tau = 27AC/8B^2$ is effective dimensionless temperature, $\xi = \sqrt{27L_1C/8B^2}$ is the nematic coherence length.[25,26] In these dimensionless units, the fluid undergoes a first-order isotropic–nematic transition at $\tau = 1/8$. The isotropic phase becomes unstable for $\tau < 0$. The scalar nematic order

parameter in bulk is given by $\hat{S}_b = (3\sqrt{6}/16)(1 + \sqrt{1 - 64\tau/9})$. Throughout this paper, the quantities appearing with a hat are rescaled with respect to the the radius of the particles, *e.g.* $d\hat{V} = R^{-3}dV$, $\hat{\xi} = R^{-1}\xi$ and $\hat{\partial}_k = R\partial_k$. Following the related previous studies,[15,25,26] the dimensionless temperature and length scales were set to $\tau = (3\sqrt{6} - 8)/12$ and $\hat{\xi} = 0.03$ respectively. This choice of parameters does closely match the parameters of the widely used liquid crystal mesogen 5CB and results in formation of stable topological defects.[25,26]

2.3 The surface free energy

As mentioned in the introduction, the normal anchoring can be modeled with much more ease[27,28] compared to the planar degenerate anchoring due to uniqueness of the orientation of nematic fluid at the colloidal surfaces.

Fournier and Galatola[24] have recently introduced a two-parameter surface energy functional that is bounded from below and assumes its minimum in the manifold of degenerate planar configurations. The surface energy consists of two terms, controlling the planar anchoring and fixing the scalar order parameter on the surface. Since we expect the formation surface topological (*e.g.* two surface defects of charge +1/2 in case of a single colloid), we relax the second constraint like previous studies,[20] resulting in the following single parameter surface energy functional:

$$F_s = W\int_{\partial\Omega} dA\left(\tilde{Q}_{ij} - \tilde{Q}^{\perp}_{ij}\right)\left(\tilde{Q}_{ji} - \tilde{Q}^{\perp}_{ji}\right) \quad (5)$$

where $\tilde{Q}_{ij} = Q_{ij} + S\delta_{ij}/3$, $\tilde{Q}^{\perp}_{ij} = (\delta_{ik} - \hat{\nu}_i\hat{\nu}_k)\tilde{Q}_{kl}(\delta_{lj} - \hat{\nu}_l\hat{\nu}_j)$ is the projection of $\tilde{Q}_{ij}$ onto the tangent plane of the surface, and $\hat{\nu}$ is the normal to the surface. W is positive and controls the stiffness of anchoring. The surface energy can be written in dimensionless variables:

$$\hat{f}_s = \frac{F_s}{f_0 R^3} = \frac{w}{R}\int_{\partial\Omega} d\hat{A}\left(\tilde{q}_{ij} - \tilde{q}^{\perp}_{ij}\right)\left(\tilde{q}_{ji} - \tilde{q}^{\perp}_{ji}\right) \quad (6)$$

where $w = 27WC/8B^2$, $\tilde{q}_{ij} = (4B/3\sqrt{6}C)^{-1}\tilde{Q}_{ij}$, $\tilde{q}^{\perp}_{ij} = (\delta_{ik} - \hat{\nu}_i\hat{\nu}_k)\tilde{q}_{kl}(\delta_{lj} - \hat{\nu}_l\hat{\nu}_j)$ and $d\hat{A} = R^{-2}dA$. We chose $\hat{w} = 0.0156$, which describes strong planar anchoring to the surface once we take the bulk free energy parameters into account.

3 Numerical minimization of the free energy

We adopt a finite element method (FEM) approach to minimize the free energy functional described in the preceding sections. The nematic cell was decomposed into tetrahedral elements by using the automatic mesh generator *Gmsh*.[29] In order to capture a more accurate representation of the curved surfaces and to provide increased numerical accuracy near the topological defects which are expected to be formed on or in the vicinity of the surfaces, a finer mesh size of $L_{SMS} = 0.025R$ was used near the spherical boundaries. We note that since the nematic coherence length is $\xi = 0.03R$, the physics of elastic deformations can be properly captured in the used mesh. The mesh size was increased to $L_{LMS} = 0.25R$ away from the particles in order to reduce the computational cost (see Fig. 2). The tensor order parameter was linearly interpolated within each of elements in the evaluation of the free energy integrals. We note that linear interpolation is the simplest scheme that preserves the properties of Q as an order tensor. For each configuration of the particles, the total dimensionless free energy was minimized using a conjugate gradient (CG) method,[30] yielding the effective potential energy (EPE) $U(d, \theta)$. In order to accelerate the minimization procedure for any given (θ, d), we used the relaxed director profile from the closest preceding configuration as the initial guess. The configuration space of the particles was scanned in the range $2.10R \le d \le 3.5R$ and $0^\circ \le \theta \le 90^\circ$ in steps of $0.05R$ and 2° respectively. For larger separations, $3.5R < d \le 6.0R$, we scan with larger θ steps of 10°. For each configuration, the minimization procedure was stopped when the relative free energy improvements dropped below 10^{-5}. We present and discuss the results in the next section.

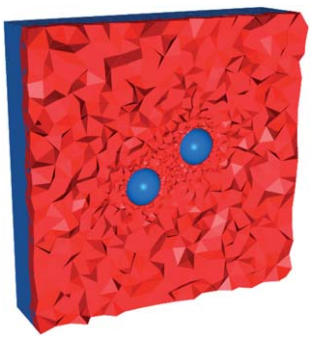

Fig. 2 A typical tetrahedral mesh used in the FEM analysis. The mesh is finer near the colloidal surfaces to capture a more accurate representation of the curved surfaces and to provide increased numerical accuracy near the topological defects.

4 Results and discussion

Fig. 3 shows the full equilibrium free energy landscape of the system. The smooth contour plot of the free energy landscape is shown in Fig. 4 for better clarity. The normal to the contour lines specify the direction of the net force between the colloidal particles. The effective potential energy of the system of two colloids is also shown in Fig. 5 as a function of the particles separation d, for four different orientations. The figure shows that for $\theta = 90^\circ$, the particles repel each other in the whole range

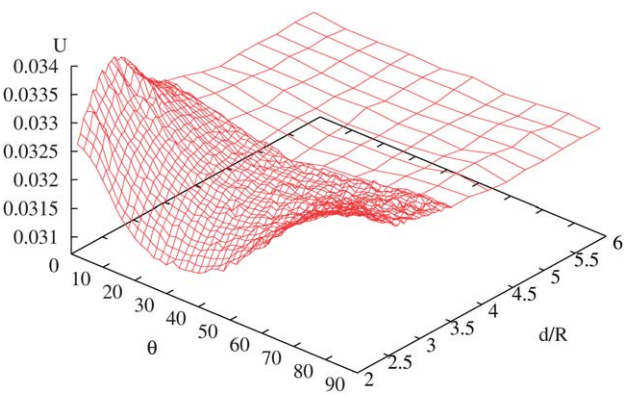

Fig. 3 The free energy landscape of the system of two particles as a function of the inter-particle distance, d/R, and θ, the angle between the line joining the center of particles and the far-field director.

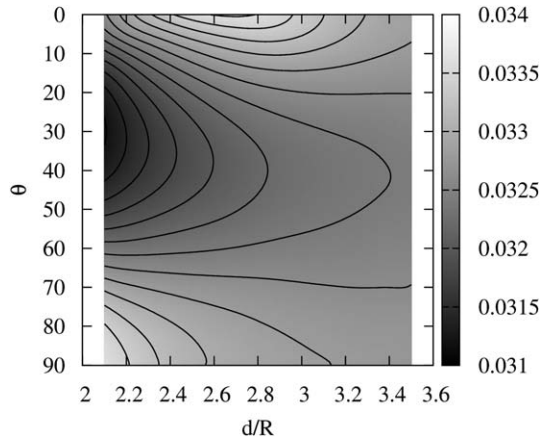

Fig. 4 The contour plot of the EPE between two particles as a function of the inter-particle distance, d/R, and θ, the angle between the line joining the center of particles and the far-field director.

of inter-particle separations, while they attract each other at $\theta = 60^\circ$ and $\theta = 30^\circ$, with a stronger attraction in the later case. This uniform attractive or repulsive behavior is destroyed for configurations with smaller angles. In particular, in the case of $\theta = 0$, the particles attract each other in the close-contact regime, $d \lesssim 2.7R$, while they repel each other for the larger separations. We will show later that this peculiar behavior is associated to the spontaneous broken axial symmetry of the defect pairs.

In order to analyze the distance dependence of the effective potential, we have fitted a two-parameter function $c_0 + c_1(d/R)^{c_2}$ to the plots of Fig. 5. The fits are shown in Fig. 6 and correspond to exponents $c_2 = -5.6 \pm 0.2$ and $c_2 = -5.7 \pm 0.2$ for $\theta = 0^\circ$ and $\theta = 90^\circ$ respectively. It is noticed that exponents are slightly larger in magnitude in comparison to the weak anchoring analytical analysis,[8] $c_2^{\text{weak}} = -5$. The exponent is $c_2 = -2.5 \pm 0.4$ for $\theta = 60^\circ$, which describes a deformation field of longer range in contrast to the weak anchoring theory. Finally, in the case $\theta = 30^\circ$, the exponent is in agreement with the analytical prediction, $c_2 = -5.0 \pm 0.2$.

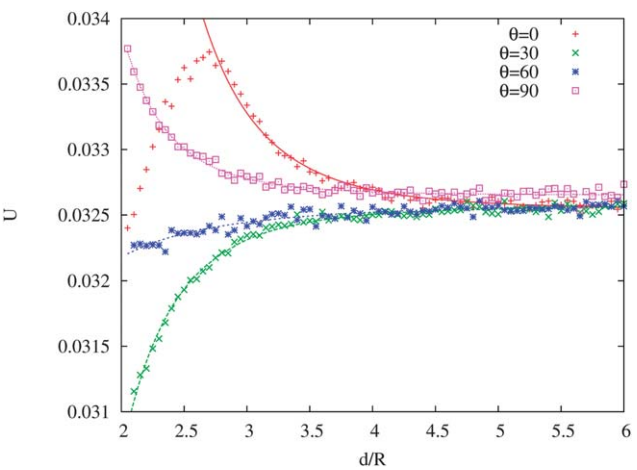

Fig. 5 Effective potential energy between two particles as a function of the inter-particle distance, d/R, for four different orientations $\theta = 0^\circ$, 30°, 60° and 90°.

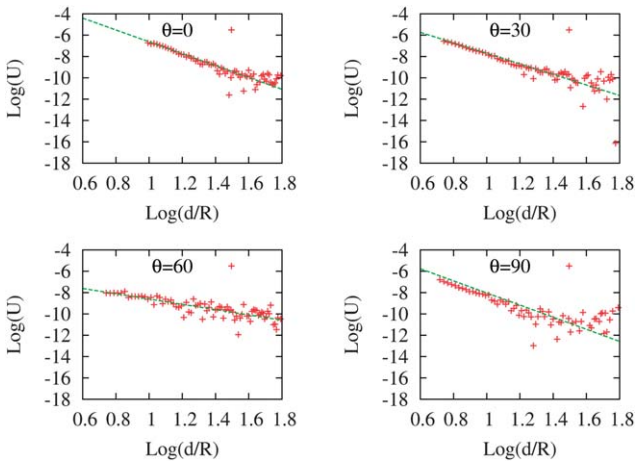

Fig. 6 Log-log plots of the effective potential energy *vs.* inter-particle separation shows an orientation-dependent asymptotic power-law behavior. Fitting a two-parameter function $c_0 + c_1(d/R)^{c_2}$ to $U(d, \theta)$, we get $c_2 = -5.7 \pm 0.2$, -5.0 ± 0.2, -2.5 ± 0.4 and -5.7 ± 0.2 for $\theta = 0$, 30°, 60° and 90° respectively.

Fig. 7 shows the effective potential energy as a function of angle θ for fixed particle–particle separations ($d/R = 2.10$, 2.30, 2.50, 2.70, 2.90, 3.10, 3.30 and 3.50). It is noticed that each of the plots has a unique global minimum. Moreover, the free energy minimum, as well the orientation angle at which the minimum is achieved (θ_{min}), decreases monotonously as the particles approach each other. This behavior is shown clearly in the inset plot of Fig. 7. Extrapolating θ_{min} to the limit $d \simeq 2R$, we find that the global minimum of the free energy is achieved for $\theta = 28^\circ \pm 2^\circ$. This result is consistent with the experimental results of Poulin and Weitz,[7] Smalyukh *et al.*[4] and Kotar *et al.*[19] who find the equilibrium angle to be $\theta \simeq 30^\circ$.

The vector field of the net force between the particles can be calculated by taking the gradient of the effective potential energy.

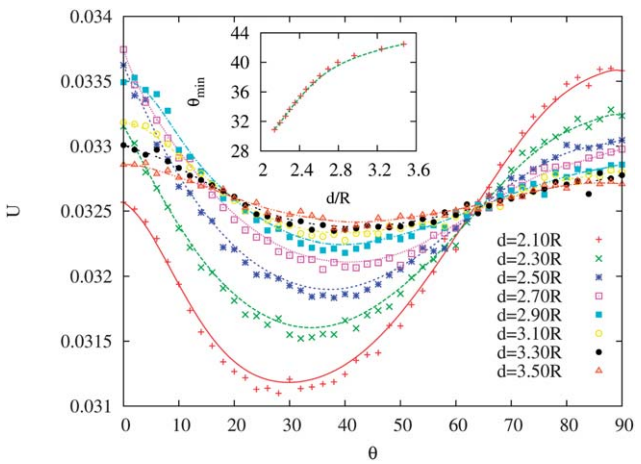

Fig. 7 Effective potential energy as a function of angle θ for different inter-particle separations $d/R = 2.10$, 2.30, 2.50, 2.70, 2.90, 3.10, 3.30 and 3.50. The inset plot shows the angle at which the free energy achieves its minimum, θ_{min}, as a function of inter-particle separation. The free energy assumes its global minimum at $\theta_{\text{min}} = 28^\circ \pm 2^\circ$.

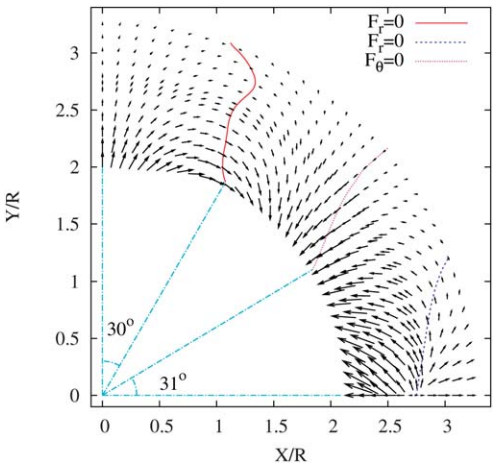

Fig. 8 The vector field of net force between two colloidal particles in the $x-y$ plane. The center of one of the particles is fixed at the origin. F_r and F_θ denote the radial and tangential components of the force, respectively.

The net force field is shown in Fig. 8 and the configurations at which the radial (F_r) and tangential (F_θ) components of the net force vanishes are indicated. It is easily noticed that the force field drives the system towards the configuration of minimum free energy, *i.e.* $\theta_{\min} \simeq 28^\circ$ and $d \simeq 2R$. The radial component of the net force is positive for $\theta \gtrsim 60^\circ$ and thus, the force is repulsive. The angle at which the radial component of net force changes sign depends on the inter-particle separation and varies in the range $60^\circ < \theta < 70^\circ$ for the investigated configurations. Repulsive interaction is expected to show up when $\theta > 75^\circ$ in quadrupolar approximation.[4] We associate this slight discrepancy to deviations from the quadrupolar approximation.

As it was mentioned earlier in this section, the inter-particle force exhibits a non-monotonous behavior as a function of inter-particle separation for small angles ($\theta \lesssim 15^\circ$). This behavior can be seen in Fig. 5, 4 and 8. In particular, for $\theta = 0^\circ$, the net force is repulsive for large separations, while it becomes attractive for $\sim d/R \lesssim 2.7$. To our knowledge, this peculiar behavior has not been studied theoretically elsewhere.

Moreover, its experimental observation requires measurement of the interaction force in separations smaller than those reported in the experimental paper by Smalyukh *et al.*[4,31] We note that precise experimental measurement of this phenomenon can be carried out by fixing the orientation of the colloidal particles by using line optical tweezers.[32]

In order to gain insight into this phenomenon, we study the configuration of the topological defects at different inter-particle separations, as shown in Fig. 9. When the particles are well separated ($d/R \gtrsim 3$), the boojum defects are aligned on the x-axis and the defect-particle pairs have a quadrupolar symmetry for each of the colloidal particles. The repulsion in this regime is thus associated to the head-to-head interaction of defects of equal charge +1/2 (Fig. 9a). When particles approach each other, the continuous $O(2)$ symmetry of the defect pairs is continuously broken due to the strong repulsion between the approaching boojums, driving them away from the axis of symmetry (Fig. 9b–c). The nematic director profile on the front and back of the colloidal particles is shown in Fig. 10a and 10b respectively, as seen along the x-axis. It is noticed that the approaching pair of

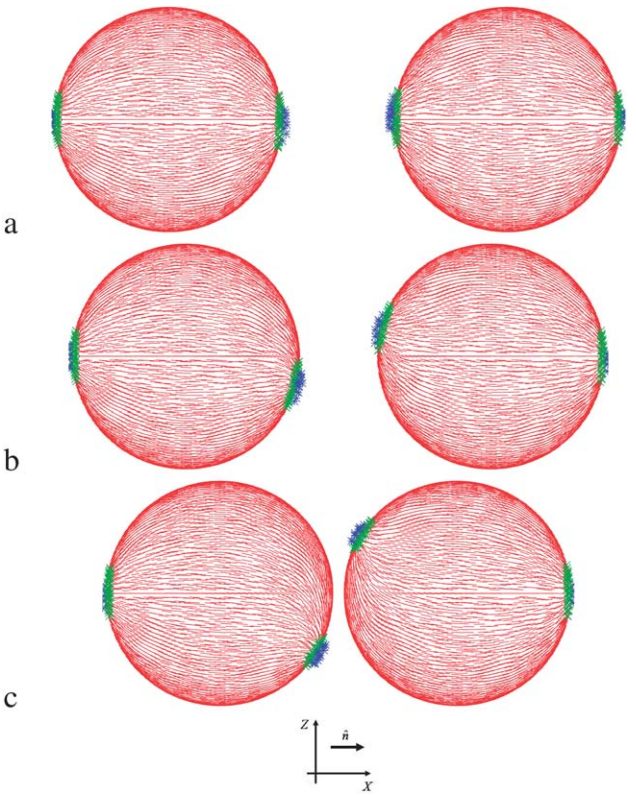

Fig. 9 Director profile and topological defects on the surface of the colloidal particles when they approach each other along the nematic direction ($\theta = 0$) at different inter-particle separations (a) $d/R = 3.00$, (b) $d/R = 2.70$, and (c) $d/R = 2.10$. The regions where the scalar order parameter drops below $0.6S_b$ are highlighted, signaling the existence of a topological defect. The defect points on the surface and bulk are indicated by dark colors, respectively.

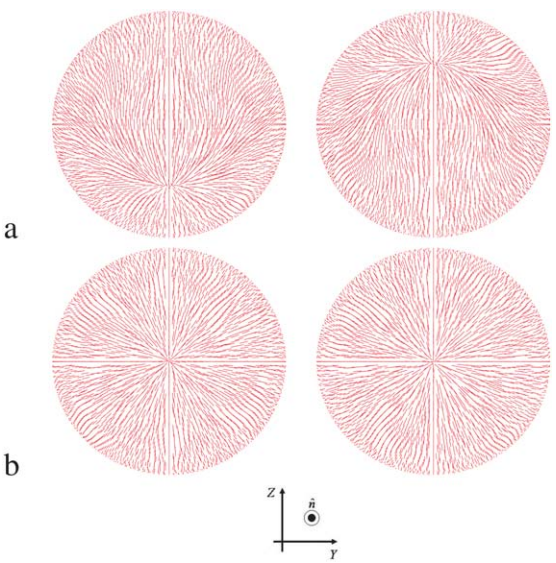

Fig. 10 Director profiles on the surface of the colloids for $\theta = 0$ and $d = 2.10R$, viewed along the x-axis. (a) Front view (near boojums) (b) back (far boojums). The displacement of approaching boojums from the x-axis is clearly noticeable.

boojums are driven away from the x-axis (Fig. 10a), while the boojums on the back of the particles remain on the x-axis. The displacement of the approaching pair of boojums induces an attraction between the colloidal particles due to the energetic tendency to reduce the volume of the distorted region between the particles.

At larger angles ($\theta \gtrsim 30°$), the axial symmetry of the defect-pair on each of the particles is almost preserved in the whole range of inter-particle separations (see Fig. 11 and Fig. 12). Therefore, the monotonous attractive or repulsive interaction at larger angles can be explained by merely taking into account the quadrupolar deformation field of each of the particles.[8]

We finally remark that although the calculations were carried out for a specific choice of bulk and surface energy parameters, we expect our results to be insensitive to variations in the parameters as long as they describe the same ($R \gg \xi$, and strong anchoring).

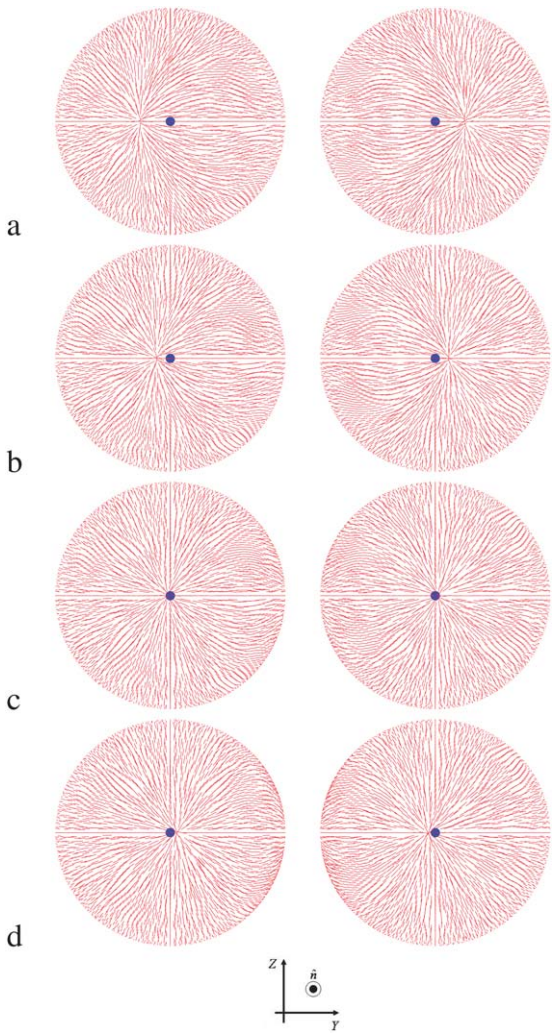

Fig. 11 Director profiles on the surface of the colloids for a center separation of $d/R = 2.10$, and for four different orientations (a) $\theta = 20°$, (b) $\theta = 30°$, (c) $\theta = 40°$ and (d) $\theta = 50°$. The spheres are viewed along the bulk nematic director and from the side where the boojums are closer to each other. The center of each of the spheres is indicated by a dot. It is noticed that the axial symmetry of the defect-pair on each of the spheres is essentially preserved.

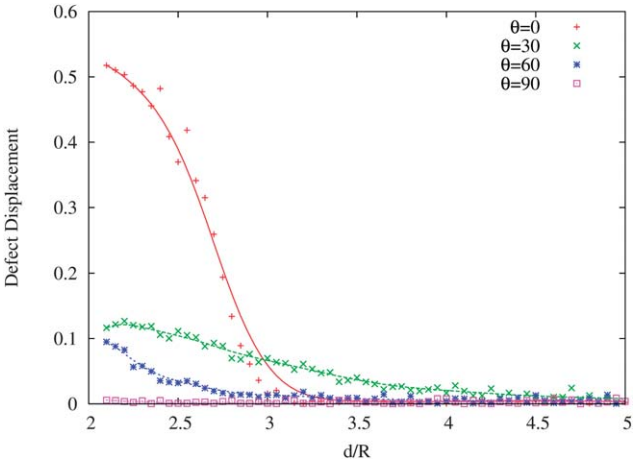

Fig. 12 Defect displacement as a function of inter-particle distances for $\theta = 0°$, 30°, 60° and 90°. Displacements are scaled to the particle radius. It shows that defects do not move a lot for large angles. The curves are guides for the eye.

5 Conclusions

In this paper, we studied the interaction of two spherical colloidal particles with degenerate planar anchoring in a nematic media by numerically minimizing the Landau–de Gennes[23] bulk and Fournier and Galatola[24] surface energy using a finite element method. Our choice of parameters belong to the regime of large particles (in comparison to the nematic coherence length) and strong surface anchoring. We obtained the nematic-induced effective potential energy of the system for different inter-particle separations and orientations with respect to the bulk nematic director.

By studying the free energy landscape of the system, we found that the system assumes its unique global minimum of energy when the particles are in close contact and are oriented at an angle $\theta = 28° \pm 2$ with respect to the bulk nematic director. Our results are in a very close agreement with the experimental results in ref. 4, $\theta \simeq 30°$. To the best of our knowledge, we have provided the first clear theoretical explanation of these experimental findings.

Our results suggest that for large inter-particle separations, the quadrupolar structure of the defect-pair on each of the particles is essentially preserved, resulting in a monotonous attractive or repulsive inter-particle net force, depending on the orientation angle. However, for smaller orientation angles ($\theta \lesssim 15°$) and at smaller inter-particle separations, the axial symmetry of the defect-pairs is continuously broken, resulting in the emergence of an attractive interaction due to the tendency of the system to reduce the volume of distorted fluid. This very unexpected attraction, in very short distances, has not been reported before and may be of interest to be explored experimentally too.

The finite element method, used in this study, can be extended to more complicated geometries. Inter-particle interaction for nonspherical colloids with planar anchoring[33] and also many-body interactions between the colloids in colloidal aggregations[34,35] are in the direction of our future studies.

Acknowledgements

We would like to thank Seyyed Mehdi Fazeli, Maryam Saadatmand, Ivan Smalyukh and Yasuyuki Kimura for their valuable comments and discussions. MRE acknowledges the Center of Excellence in Complex Systems and Condensed Matter (CSCM) for partial support.

References

1 P. Poulin, H. Stark, T. C. Lubensky and D. A. Weitz, *Science*, 1997, **275**, 1770.
2 V. G. Nazarenko, A. B. Nych and B. I. Lev, *Phys. Rev. Lett.*, 2001, **87**, 075504.
3 M. Yada, J. Yamamoto and H. Yokoyama, *Phys. Rev. Lett.*, 2004, **92**, 185501.
4 I. I. Smalyukh, O. D. Lavrentovich, A. N. Kuzmin, A. V. Kachynski and P. N. Prasad, *Phys. Rev. Lett.*, 2005, **95**, 157801.
5 I. Musevic, M. Skarabot, U. Tkalec, M. Ravnik and S. Zumer, *Science*, 2006, **313**, 954.
6 J. Fukuda, *J. Phys. Soc. Jpn.*, 2009, **78**, 041003.
7 P. Poulin and D. A. Weitz, *Phys. Rev. E: Stat. Phys., Plasmas, Fluids, Relat. Interdiscip. Top.*, 1998, **57**, 626.
8 R. W. Ruhwandl and E. M. Terentjev, *Phys. Rev. E: Stat. Phys., Plasmas, Fluids, Relat. Interdiscip. Top.*, 1997, **55**, 2958.
9 T. C. Lubensky, D. Pettey, N. Currier and H. Stark, *Phys. Rev. E: Stat. Phys., Plasmas, Fluids, Relat. Interdiscip. Top.*, 1998, **57**, 610.
10 H. Stark, *Phys. Rep.*, 2001, **351**, 387.
11 B. I. Lev, S. B. Chernyshuk, P. M. Tomchuk and H. Yokoyama, *Phys. Rev. E: Stat. Phys., Plasmas, Fluids, Relat. Interdiscip. Top.*, 2002, **65**, 021709.
12 O. Guzman, E. B. Kim, S. Grollau, N. L. Abbott and J. J. de Pablo, *Phys. Rev. Lett.*, 2003, **91**, 235507.
13 D. Andrienko, M. Tasinkevych, P. Patrício, M. P. Allen and M. M. T. da Gama, *Phys. Rev. E: Stat. Phys., Plasmas, Fluids, Relat. Interdiscip. Top.*, 2003, **68**, 051702.
14 N. M. Silvestre, P. Patrício, M. Tasinkevych, D. Andrienko and M. M. T. da Gama, *J. Phys.: Condens. Matter*, 2004, **16**, S1921.
15 M. Ravnik, M. Skarabot, S. Zumer, U. Tkalec, I. Poberaj, D. Babic, N. Osterman and I. Musevic, *Phys. Rev. Lett.*, 2007, **99**, 247801.
16 A. Fernandez-Nieves, V. Vitelli, A. S. Utada, D. R. Link, M. Marquez, D. R. Nelson and D. A. Weitz, *Phys. Rev. Lett.*, 2007, **99**, 157801.
17 J. Fukuda and H. Yokoyama, *Phys. Rev. Lett.*, 2005, **94**, 148301.
18 K. Takahashi, M. Ichikawa and Y. Kimura, *Phys. Rev. E: Stat., Nonlinear, Soft Matter Phys.*, 2008, **77**, 020703.
19 J. Kotar, M. Vilfan, N. Osterman, D. Babic, M. Copic and I. Poberaj, *Phys. Rev. Lett.*, 2006, **96**, 207801.
20 M. Vilfan, N. Osterman, M. Copic, M. Ravnik, S. Zumer, J. Kotar, D. Babic and I. Poberaj, *Phys. Rev. Lett.*, 2008, **101**, 237801.
21 A. B. Nych, U. M. Ognysta, V. M. Pergamenshchik, B. I. Lev, V. G. Nazarenko, I. Musevic, M. Skarabot and O. D. Lavrentovich, *Phys. Rev. Lett.*, 2007, **98**, 057801.
22 I. I. Smalyukh, S. Chernyshuk, B. I. Lev, A. B. Nych, U. Ognysta, V. G. Nazarenko and O. D. Lavrentovich, *Phys. Rev. Lett.*, 2004, **93**, 117801.
23 P. G. de Gennes and J. Prost, *The Physics of Liquid Crystals*, 2nd ed., Clarendon Press, Oxford, 1993.
24 J. B. Fournier and P. Galatola, *Europhys. Lett.*, 2005, **72**, 403.
25 J. Fukuda, H. Stark, M. Yoneya and H. Yokoyama, *Phys. Rev. E: Stat., Nonlinear, Soft Matter Phys.*, 2004, **69**, 041706.
26 J. Fukuda, H. Yokoyama, M. Yoneya and H. Stark, *Mol. Cryst. Liq. Cryst.*, 2005, **435**, 723.
27 A. Rapini and M. Popoular, *J. Phys. (France)*, 1969, **30**, 54.
28 M. Nobili and G. Durand, *Phys. Rev. A: At., Mol., Opt. Phys.*, 1992, **46**, R6174.
29 C. Geuzaine and J.-F. Remacle, *Gmsh: a three-dimensional finite element mesh generator with built-in pre- and post-processing facilities*.
30 W. H. Press, S. A. Teukolsky, W. T. Vetterling and B. P. Flannery, *Numerical Recipes*, Cambridge University Press, 2nd ed., 1992.
31 Upon the completion of this work, it was brought to our attention in a private communication with Ivan Smalyukh that they had observed displacement of the topological defects in their experiments.
32 Private communications with Yasuyuki Kimura.
33 C. P. Lapointe, T. G. Mason and I. I. Smalyukh, *Science*, 2009, **326**, 1083.
34 M. Tasinkevych and D. Andrienko, *Eur. Phys. J. E: Soft Matter Biol. Phys.*, 2006, **21**, 277.
35 T. Araki and H. Tanaka, *Phys. Rev. Lett.*, 2006, **97**, 127801.